Structure and Dynamics of Cl and Br Ions and Atoms in Xe Clusters

Yehuda Zeiri

Department of Chemistry, NRCN, P.O. Box 9001, Beer-Sheva 84190, Israel

Received: September 30, 1997; In Final Form: December 31, 1997

A genetic algorithm based search method was used to identify the lowest energy structure of Xe_nY ($Y = Cl^-$, Br^-, Cl, and Br) microclusters. The optimization was performed using an empirical potential constructed from pairwise interactions (for the neutral clusters) together with three-body terms in the case of ionic systems. The variation of the cluster energy and the electrostatic stabilization energy as a function of the cluster size, $n = 1-16$, was examined. The calculations indicate that for large n values both Cl and Cl^- were located inside the Xe cluster, while Br and Br^- adsorb onto the cluster surface. For most cluster sizes, the lowest energy structures of the lighter halogen seem to be independent of its charge state. However, markedly different structures were obtained in the case of Br^- and Br. The stabilization energies, E_{stab}, for the charged clusters were estimated using the most stable structures found in the optimizations. Both halogens exhibit rapid linear increase of the stabilization energy with cluster size up to $n = 6$. For larger clusters E_{stab} continues to increase linearly as a function of n but with a much smaller rate. The time evolution of the Xe_nY^- clusters after photoionization was simulated using molecular dynamics. It was found that for Cl^-, the loss of the stabilization energy did not lead to appreciable fragmentation of the parent cluster, while for bromine a high degree of fragmentation occurs in less than 100 ps.

I. Introduction

The investigation of the structure and dynamics of small clusters is important since these systems serve as a bridge between the gas phase and the solid state. In addition, study of the interaction between microclusters and various molecules or ions may make a major contribution to our understanding of solvation processes. These reasons motivated the development of suitable experimental and theoretical methods to explore such systems. The structures of weakly interacting atomic systems, such as clusters of rare-gas atoms, have been the subjects of investigation during the past three decades.[1] The forces between the atoms in these systems are well described by simple two-body interaction potentials. The contribution of three-body terms to the full many-body potential of these clusters appears to be unimportant for most calculations.[2] Hence, reliable simulations of the structure and dynamics of these systems using a variety of theoretical approaches can be achieved. However, if the investigated system contains ionic species, the inclusion of three-body terms in the description of their potential surface seems to be unavoidable. The properties of microclusters were examined using a variety of theoretical methods, the two most important ones being molecular dynamics (MD)[3] and simulated annealing.[4]

The theoretical studies were triggered in recent years by the development of experimental techniques that allow the measurement of observables directly related to the structure of the cluster and to reactions among different species embedded in the cluster. The evolution of cluster properties with size has been studied by both mass analysis[5] and various spectroscopic techniques.[6] In the case of charged clusters, the study of their structures and energetics was greatly advanced using photoelectron spectroscopy.[7] This approach seems to be the best suited to the investigation of negative ion−solvent interactions in clusters. Due to the vertical nature of the photodetachment process in these experiments, solvent−solvent interactions have a negligible effect on the energetics of the problem, and hence the ion−solvent interaction can be probed directly.

In this paper a detailed study of the structure and energetics of variously sized Xe_nY ($Y = Cl^-$, Br^-, Cl, and Br) will be presented. The most stable structures of these clusters (for $n = 1-16$) were identified using an optimization method that is based on genetic algorithms (GAs).[8,9] These lowest energy structures were used to calculate the electrostatic stabilization energies, E_s, of the ionic clusters and its dependence on the cluster size. Finally, the fragmentation of parent Xe_nY^- clusters following photoionization was simulated using molecular dynamics calculations.

The next section contains a brief description of the GA-based optimization method used to locate the most stable cluster structures followed by an outline of the potential function used in the calculations. The results of the simulations will be presented and discussed in section III, while the last section is devoted to conclusions.

II. Details of the Calculations

To obtain the lowest energy structure of a cluster, one has to perform a search for the global minimum of its multidimensional potential energy surface. This optimization process becomes quite difficult as the cluster size increases due to the rapidly growing number of local minima. In the present study a genetic algorithm based optimization method was used to search for the most stable cluster structure. Since this approach has been discussed in detail elsewhere,[8] only a brief description will be given below.

Genetic algorithms (GAs) are global optimization methods based on several metaphors from biological evolution. The name is derived from the ability of the algorithm to simulate selection in an evolving population of living creatures attempting

S1089-5639(97)03179-4 CCC: $15.00
Published on Web 04/02/1998

to adapt to their environment. The conventional GAs differ from traditional optimization methods in the following important respects:[10]

(a) They work using an encoding of the control variables, rather than the variables themselves. In most applications, a binary bit string (chromosome) is used for the coding of the control variables.

(b) GAs search from one population of solutions to another population, rather than from individual to individual.

(c) The GA uses only objective function information, not derivatives.

(d) GAs use probabilistic, not deterministic, transition rules.

A variety of optimization procedures that incorporate genetic algorithms are described in the literature. All these GA-based methods are constituted of the following five basic building blocks: (1) Generation of the initial population. (2) Evaluation of the fitness function for the individuals in the population. (3) Selection of "parents" from which the next generation is formed. (4) Application of the GA operators to the selected "parents" to form "sons". (5) Selection of the members for the new generation from the ensemble of "parents" and newly formed "sons".

The first step is accomplished in most cases by random selection of initial individuals. The representation of the individuals can be performed in the control variable's space (i.e., atomic coordinates in the case of cluster structure optimization) or using a predefined binary representation of the control variables. If binary representation is used, coding and decoding procedures should be defined since the fitness function is usually evaluated in the control variables space (fitness related to cluster energy in the present study). Typical population sizes are in the range of a few tens to a few hundred individuals.

Once the initial generation is formed, the fitness of each individual, F_i, is calculated. These fitness values are defined in this work as the normalized cluster energy, $F^j_i = E^j_i/E^j_{\text{best}}$. Here F^j_i and E^j_i are the fitness and energy of structure i and generation j respectively while E^j_{best} is the energy of the most stable structure in the population. According to the potential function used to evaluate the cluster energies (see below), stable clusters are associated with negative E^j_i. Hence, negative F^j_i values were set to zero. The scaling used to establish the relation between the cluster energy and its fitness determines the relative frequency with which a given individual will be used as a parent in the formation of the next generation.

To evolve the population from a given generation to the next one, a set of GA operators is applied to randomly chosen parent structures. These operations result in the formation of new structures, "sons", that may become individuals in the next generation. The two most common GA operators are "crossover" and "mutation". The first operation, crossover, involves the exchange of a randomly chosen section between two parent strings (i.e., ABCD + A′B′C′D′ → AB′C′D′ + A′BCD). The result of this operation is two new "sons". The second operation, mutation, consists of a random change of a single element in a parent string. If, for example, a binary representation is used, the mutation operation consists of randomly selecting an element in the parent string and changing its value (i.e., 0 → 1 or 1 → 0). Once the sons are formed, a selection rule is used to determine which individuals in the ensemble of sons and parents will be included in the next generation. A number of different selection rules have been described in the literature.[10] Three such rules were examined in a previous study.[8c] In this work we used the second selection rule of ref 8c, namely, a son is accepted as a member of the new generation provided its fitness is higher than that of its parent. For operations where two sons are formed, the acceptance of each one is determined by a comparison of its fitness with that of one of the parents (randomly chosen). Otherwise, the parent is transferred to the next generation. Once the new generation is constructed, the scheme described above is repeated until the convergence requirements are fulfilled.

To avoid the coding and decoding process, a GA-based optimization procedure in which the control variables are used to form the strings was formulated.[8] The main advantage of this approach is related to the high accuracy in the determination of the global minimum of the system being examined. The application of this search method was accomplished using a set of GA operators that are suited for operation on chromosomes represented by the control variables. It should be noted that the probability of using these GA operators is varied during the search process according to the success of each operator in generating high-fitness sons.

In all the calculations performed in this study we used populations of 100 individuals. The optimized structure for any given cluster represents the lowest energy configuration obtained in 50 different searches each starting from a new random initial population. The GA-based optimization method described above does not guarantee the identification of the global minimum on a complicated multi variable energy hypersurface. However, comparison of its performance with that of the simulated annealing approach shows that it is more efficient and has a highest rate of success in the location of lowest energy structures of atomic clusters.[8]

Potential Functions. As stated above, the fitness of a given atomic arrangement in the cluster is related to its potential energy, E_i. In the case of ionic clusters, Xe_nY^- (Y = Cl or Br), the potential energy was assumed to have the form

$$V = \sum_{i=1}^{n} V_{Y^- i} + \sum_{i=1}^{n-1}\sum_{j>i}^{n} V_{ij} + \sum_{i=1}^{n-1}\sum_{j>i}^{n} V_{Y^- ij} \qquad (1)$$

where the first two terms represent Xe−ion and Xe−Xe interactions respectively, while the last term comprises three-body contributions corresponding to the energy between dipoles on the Xe atoms induced by the halogen ion.[4b] In eq 1 we neglected the contribution from the full, self-consistent, many-body interactions among the induced dipoles. This approximation is justified since the polarization of the Xe atoms is dominated by their interaction with the halogen ion. Thus, the three-body terms in eq 1 are believed to constitute a quite accurate and economical (by means of computational time) model of these interactions.

For the Xe−ion interaction we adopted the form suggested by Mansky and Flannery:[11]

$$V_{Y^- i} = B\left(\frac{R_0}{R_{Y^- i}}\right)^{12} + (C - D)\left(\frac{R_e}{R_{Y^- i}}\right)^{V} - C\left(\frac{R_e}{R_{Y^- i}}\right)^{4} \qquad R_{Y^- i} \le R_e \quad (2)$$

$$= \frac{C_{12}}{{R_{Y^- i}}^{12}} - \frac{\alpha_d}{2{R_{Y^- i}}^{4}} - \frac{C_6}{{R_{Y^- i}}^{6}} - \frac{C_8}{{R_{Y^- i}}^{8}} - \frac{C_{10}}{{R_{Y^- i}}^{10}} \qquad R_{Y^- i} > R_e$$

where $V_{Y^- i}$ represents the interaction between Xe atom i and the ion Y^-. The parameters used to compute the $Xe-Br^-$ and $Xe-Cl^-$ potentials are those given in ref 11. In the second term of eq 1 a Lennard-Jones potential was used to represent

TABLE 1: Binding Energies and Equilibrium Distances for the Various Diatomic Species Used in the Simulations

molecule	*De* [eV]	*Re* [Å]
Xe−Xe	0.02432	4.3634
Xe−Br	0.02320	4.1666
Xe−Br$^-$	0.16875	3.3963
Xe−Cl	0.03464	3.3510
Xe−Cl$^-$	0.19782	3.3041

the interaction between Xe atoms i and j:

$$V_{ij} = 4\epsilon\left[\left(\frac{\sigma}{R_{ij}}\right)^{12} - \left(\frac{\sigma}{R_{ij}}\right)^{6}\right] \quad (3)$$

where the parameters for the Xe−Xe potential were taken from ref 12. The induced dipole−induced dipole interaction, the last term of eq 1, has the following form:[4b]

$$V_{Y^-ij} = \frac{q^2\alpha_i\alpha_j}{(\vec{R}_{ij}\vec{R}_{Y^-i}\vec{R}_{Y^-j})}\left\{\vec{R}_{Y^-i}\cdot\vec{R}_{Y^-j} - \frac{3(\vec{R}_{Y^-i}\cdot\vec{R}_{ij})(\vec{R}_{Y^-j}\cdot\vec{R}_{ij})}{\vec{R}_{ij}^{\,2}}\right\} f_c(R_{ij}) \quad (4)$$

with

$$f_c(R_{ij}) = (1 + e^{-b_c(R_{ij}-R_c)})^{-1} \quad (5)$$

where the Xe polarizabilities used in eq 4 were identical to those in eq 2. The parameters used in the switching function of eq 5 were $b_c = 10$ Å^{-1} and $R_c = 2.321$ Å.

In the case of neutral Xe$_n$−halide clusters, the potential energy was calculated as a sum of pairwise interactions of the form

$$V = \sum_{i=1}^{n} V_{Yi} + \sum_{i=1}^{n-1}\sum_{j>i}^{n} V_{ij} \quad (6)$$

where the second term on the right-hand side represents the Xe−Xe interaction (as in eq 1) and the first term represents the interaction between the halogen atom and the Xe atoms. In the case of Xe−Cl we used the exp−6 form suggested in ref 14:

$$V = Ae^{-br} - C_6/R_{Yi}^{\,6}$$

while for Xe−Br the interaction was assumed to be given by a Lennard-Jones (12−6) potential. The parameters for the Xe−Br potential were obtained using the Lorentz−Berthelot combining rules; the parameters related to the Xe−Xe and Br−Br interactions were taken from refs 12 and 14, respectively. These combining rules were employed in recent studies of similar systems.[13,16] It is recognized that the functional forms chosen to represent the Xe−Cl and Xe−Br interactions are not the most suitable forms for open-shell systems. However, we believe that these forms provide an accurate description of binding energies, *De*, and equilibrium distances, *Re*, of the Xe−Cl and Xe−Br species. As we shall see below, the relative magnitudes of the binding energies and the equilibrium distances have important ramifications regarding the lowest energy structures and stabilization energies of the clusters examined. The functional forms of these interaction potentials are expected to have a much smaller influence on these quantities. However, even if the interaction potentials used to describe the Xe−Cl and Xe−Br bonds are inaccurate, one can view this study as a "model study" which, as we shall see below, leads to interesting results. The binding energies and equilibrium distances of the various diatomic species are summarized in Table 1.

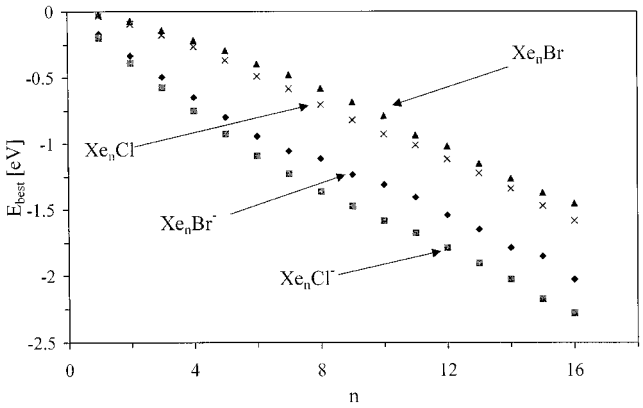

Figure 1. Variation of the most stable cluster energy, E_{best}, as a function of cluster size.

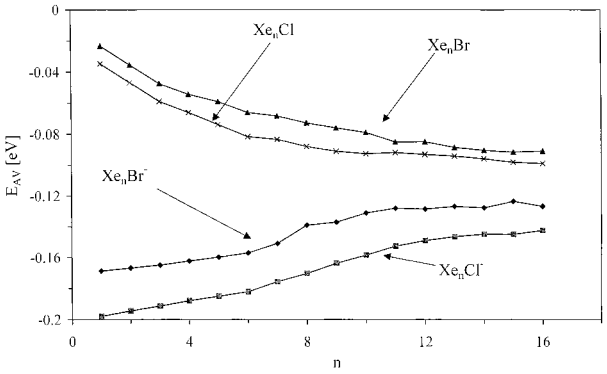

Figure 2. Variation of the average energy per atom, $E_{av} = E_{best}/n$, as a function of cluster size.

The potential functions described in this section were used to evaluate the potential energy of a given structure, E_i. The cluster energies were converted into fitness values by normalizing E_i by the value of the lowest energy structure in the population. It should be noted that the cluster energy is measured with respect to the energy of infinitely separated particles. Thus, negative cluster energies are associated with bonded structures while positive energy values are associated with unstable clusters.

III. Results and Discussion

The GA-based optimization method was used to search for the most stable structures of the Xe$_n$Y$^-$ and Xe$_n$Y (where Y = Cl, Br and $n = 1-16$) clusters. The variation of the calculated energies of the lowest energy structures, E_{best}, as a function of cluster size is shown in Figure 1. The data shown exhibits a monotonic decrease of E_{best} (increasing stability) as a function of n for the neutral clusters. In the case of the ionic clusters E_{best} changes linearly as a function of n. Careful examination of the results for ionic clusters shows a change in the rate of E_{best} decrease at approximately $n = 6-8$. For small n values the variation of E_{best} is determined by the number of Xe atoms in the cluster which are nearest neighbors of the halogen ion. Such monotonic variation of E_{best} for the different cluster types is anticipated. Moreover, the average energy of a cluster atom, $E_{av} = E_{best}/n$, is expected to decrease as a function of the cluster size (for small clusters). This decrease of E_{av} is not expected to be linear in n, since the number of new pair interactions formed upon the inclusion of an additional Xe atom changes with the cluster size and its structure. The variation of E_{av} as a function of n is shown in Figure 2 for the four cluster types investigated. The anticipated behavior of E_{av} is clearly observed

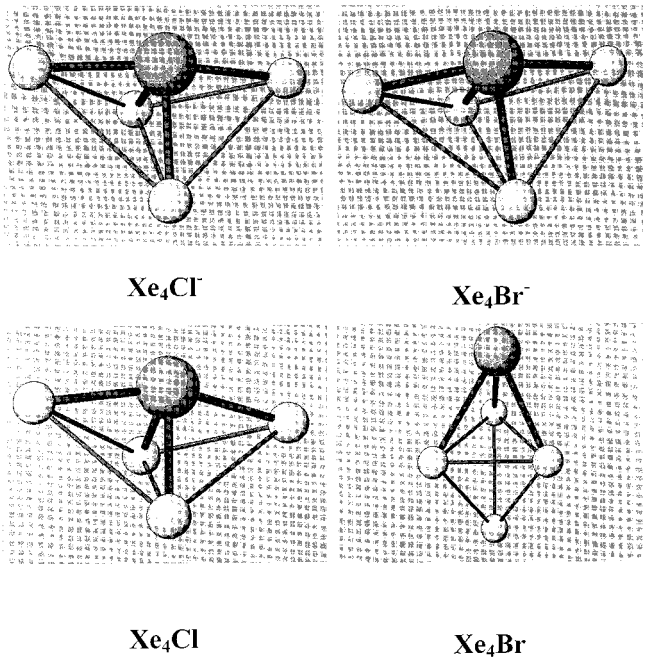

Figure 3. Lowest energy structures of Xe_4Y clusters obtained by the GA-based optimization. Structure in the upper left panel corresponds to $Y = Cl^-$, the upper right to $Y = Br^-$, the bottom left to Y = Cl and the bottom right to Y = Br. In all four cases, the large dark ball represents the halogen ion or atom, while small light balls correspond to Xe atoms.

for the neutral clusters. In this case the decrease of E_{av} as a function of n is rapid for small clusters and seems to tend to a constant value for large n values. A constant E_{av} value is expected for large clusters, where the addition of a Xe atom results in a nearly constant number of newly formed bonds. Contrary to the behavior observed in neutral clusters, in the case of Xe_nY^- E_{av} exhibits an initial increase but nonetheless tends to a constant rate of change for larger cluster sizes. The increase in the magnitude of E_{av} for small n values is related to the repulsion induced by the three-body terms used in the evaluation of the cluster energy (see eq 1). For small clusters the magnitude of this repulsion is larger than the gain in energy due to the attractive Xe−Xe interactions, and it results in the observed initial increase in E_{av}. Once the cluster is large enough, the repulsion converges to a constant value and E_{av} becomes nearly independent of n. These results clearly demonstrate the importance of the inclusion of three-body interaction terms in the potential function describing charged cluster energies.

Next we examine the structure of the lowest energy clusters obtained in the optimization process. The most stable cluster structures of the four cluster types which were obtained for n = 4, 6, 8, 10, and 13 are presented in Figures 3−7. In all cases the top pair correspond to the ionic clusters, Xe_nBr^- (right) and Xe_nCl^- (left), while the pair at the bottom to the neutral ones, Y = Br (right) and Y = Cl (left). For all the structures shown bonds were drawn only between nearest-neighbor pairs where the distance between the two particles was equal to the equilibrium separation of the pair considered. Examination of these results shows some general trends. For example, for all n values both ionic and neutral chlorine-containing clusters exhibit identical structures (on the basis of cluster symmetry and the position of the halogen atom/ion). The corresponding bromine-containing clusters show a quite different behavior. Moreover, comparison of the structures obtained for the two halogens shows marked differences in symmetry and the position of the halogen. These characteristics of the clusters

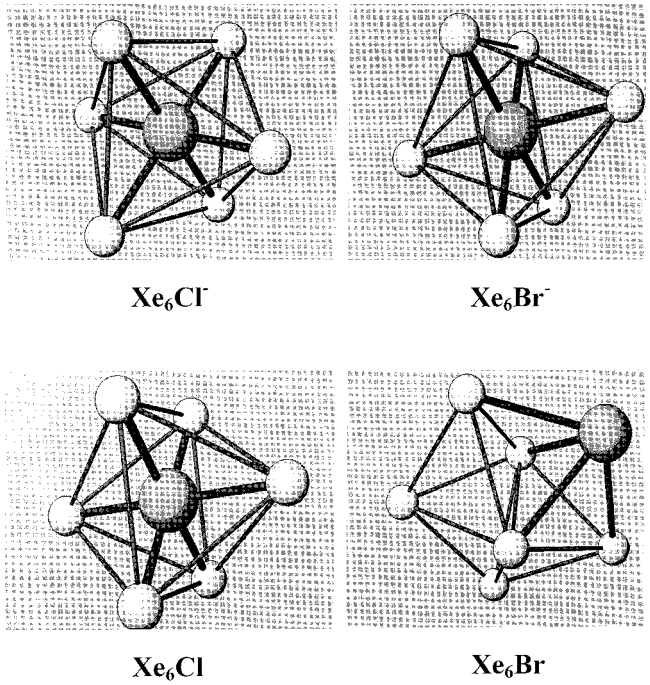

Figure 4. As in Figure 3, but for Xe_6Y.

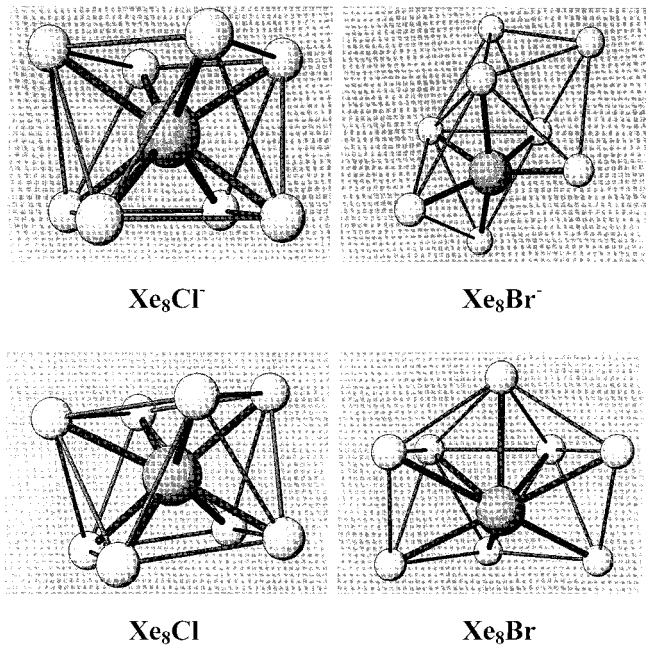

Figure 5. As in Figure 3, but for Xe_8Y.

can be related to the differences between the binding energies and the equilibrium distances of the particles forming the clusters.

In the case of chlorine, the binding energies of both Xe−Cl and $Xe-Cl^-$ are larger than that of Xe−Xe, while their equilibrium bond distances are smaller than that of Xe−Xe. Hence, the lowest-energy structure will correspond to the largest possible number of Xe−halogen bonds in the cluster. The results presented in Figures 3−7 indicate that 8 Xe atoms yield the largest possible number of nearest-neighbor Xe−halogen pairs. A larger number of Xe atoms will result in a Xe−Xe repulsion that is not compensated by the additional Xe−halogen binding. Thus, the first "solvation" shell, in this case, contains 8 Xe atoms. Increasing n beyond $n = 8$ leads to the growth of additional shells which correspond to larger Xe−halogen

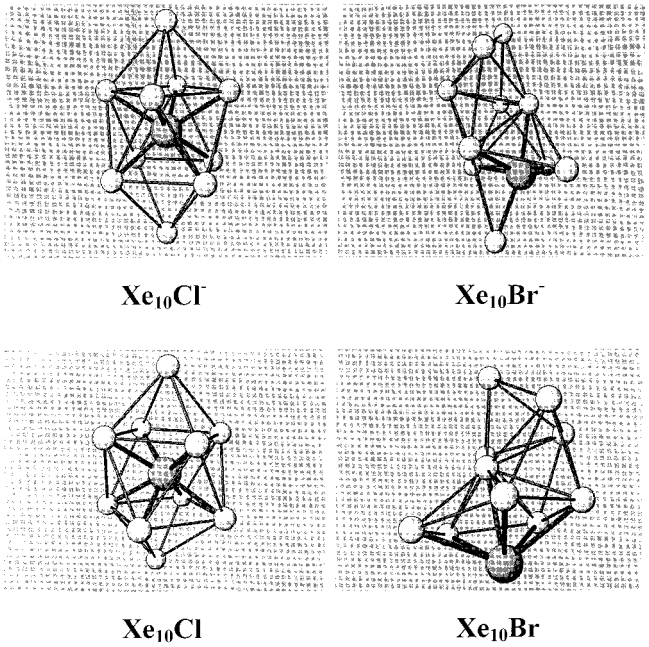

Figure 6. As in Figure 3, but for $Xe_{10}Y$.

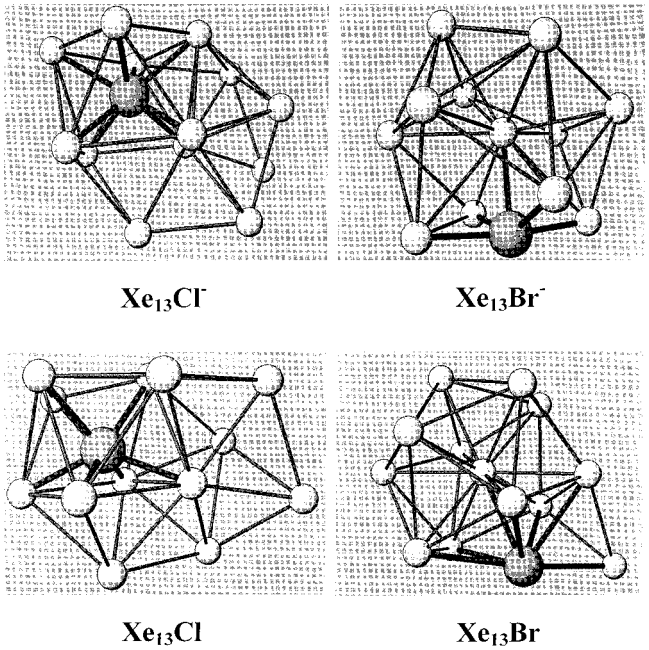

Figure 7. As in Figure 3, but for $Xe_{13}Y$.

distances. The outcome of this interplay between binding energies and equilibrium distances is that the chlorine (atom or ion) tends to be positioned **inside** the Xe cluster.

The binding energies of $Xe-Cl^-$ is larger than that of $Xe-Br^-$, and hence it is expected that the number of nearest-neighbor Xe atoms about the Br^- ion, N_{sol}, will be smaller than the corresponding number for Cl^-. Indeed, the inner "solvation" shell for Br^- contains, in most cases, only 6 Xe atoms. The exceptional cases are $Xe_{12}Br^-$ and $Xe_{13}Br^-$ where $N_{sol} = 7$ and 5, respectively. This variation in N_{sol} is related to the interplay between the repulsive and attractive interactions in the different arrangements of the particles in the cluster. In this case, increasing n beyond 6 results in the growth of a bulklike Xe structure with the bromine ion attached to its surface.

Finally, the neutral bromine clusters group is exceptional compared with the other three cluster types. In the first three

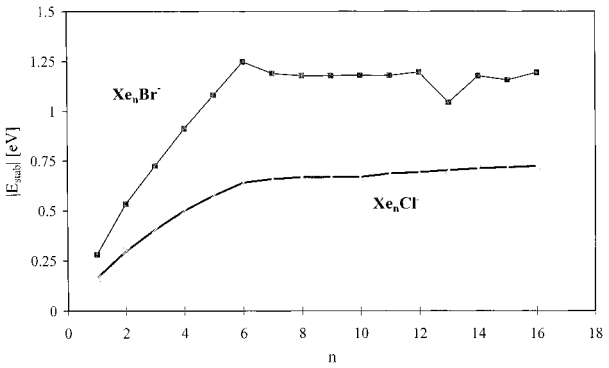

Figure 8. Variation of the stabilization energy of the two types of ionic clusters investigated as a function of cluster size.

groups the Xe−halogen bonds are much stronger than the Xe−Xe bond, while the corresponding equilibrium separations are shorter than those of Xe−Xe. These features dominated the lowest energy structures of the clusters. In the case of neutral bromine, both the Xe−Br binding energy and its equilibrium distance are very close to the corresponding values for the Xe−Xe pair. Examination of the lowest energy structures of the Xe_nBr clusters shows that N_{sol} undergoes large fluctuations in the range 3−11. Moreover, because the number of Xe−Xe interactions is maximized, the bromine is found, for all cluster sizes investigated, attached to the surface of a Xe cluster.

In summary, the comparison between the lowest energy structures of the four cluster types shows that for large n values bromine tends to be attached to the surface of a Xe cluster, while both Cl^- and Cl are imbedded inside the Xe cluster.

The utilization of photoelectron spectroscopy[7] in the study of the energetics and structures of ionic clusters has proved to be very fruitful. The vertical transition of the photodetachment process allows one to obtain by these experiments the stabilization energy, E_{stab}, of the ionic cluster compared with that of the neutral one. The magnitude of E_{stab} is defined as

$$E_{stab} = E[Xe_nY^-(\vec{R}_{min})] - E[Xe_nY(\vec{R}_{min})] \qquad (7)$$

where $\vec{R}_{min}$ represents the coordinates of the particles in the lowest energy structure of the **ionic** cluster. The variation of $|E_{stab}|$ as a function of the cluster size is shown in Figure 8. For both halogens the rapid initial increase in $|E_{stab}|$ is followed by a much slower one with the change in the rate occurring for both systems at $n = 6$. In the case of Br^-, $n = 6$ corresponds to the completion of the inner "solvation" shell. The increase in cluster size beyond $n = 6$ results mainly in the formation of additional Xe−Xe pairs whose interactions are not changed by the vertical transition during the photodetachment process. Thus, a nearly constant value of $|E_{stab}|$ is obtained for $n > 6$. The sharp decrease in the magnitude of E_{stab} for $n = 13$ is related to the variation in the size of the inner "solvation" shell for $n =$ 12, 13, and 14. The corresponding N_{sol} values obtained for these clusters are 7, 5, and 6, respectively.

In the case of Cl^--containing clusters, despite the fact that $N_{sol} = 8$, a marked change in the rate that $|E_{stab}|$ increases is observed also at $n = 6$. This change in the rate at $n = 6$ is due to the difference between the Cl^-−Xe and Cl−Xe interactions. The large initial difference between Cl^-−Xe and Cl−Xe binding energies decreases rapidly with increasing n values as a result of the repulsion due to the three-body terms. Indeed, the change of cluster energy upon addition of an extra Xe atom, $E(n) - E(n-1)$, for both ionic and neutral chlorine-containing clusters becomes nearly constant for $n > 6$.

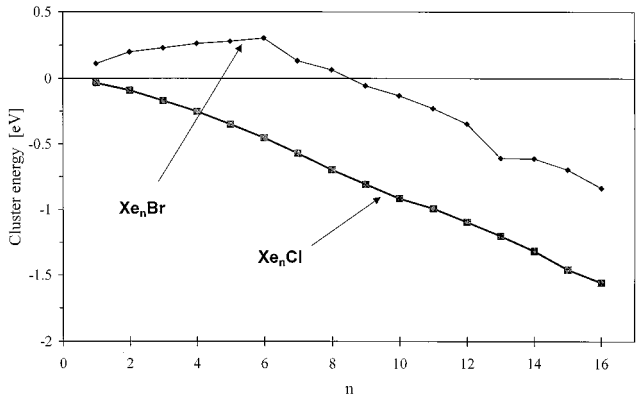

Figure 9. Variation of the energy of the neutral cluster after photoionization as a function of cluster size.

The results presented in Figure 8 show that for all n values the magnitude of $|E_{stab}|$ for the Xe_nBr^- clusters is much larger than that of the corresponding Xe_nCl^- clusters. This discrepancy is related to differences between the structures of the ionic and neutral clusters of the two halogens. In the case of chlorine, the lowest energy structures obtained for the ionic clusters are practically identical (in terms of symmetry and interparticle distances) with those of the neutral ones. As a result, the photodetachment process produces neutral clusters with structures very close to those of the most stable ones (within a few percent). Hence, the magnitude of $|E_{stab}|$ is determined by the difference in binding energy of the Cl^-−Xe bond as compared to that of Cl−Xe.

The situation in the case of the bromine-containing clusters is quite different. Here, the lowest energy structures of the ionic clusters are, for most n values, markedly different than those of the corresponding neutral clusters. Moreover, the equilibrium separation for Br^-−Xe is much smaller than that of Br−Xe. The result of these differences is that the structure of the neutral cluster formed by photoionization is substantially deformed relative to the corresponding most stable structures. Thus, in addition to the differences in the binding energies of Br^-−Xe and Br−Xe, E_{stab} in this case contains large contributions associated with structural deformations.

The differences in lowest energy cluster structures between ionic and neutral halogens (particularly in the case of Br) may result in the formation of a highly unstable neutral cluster after the photodetachment process. The variation of $E[Xe_nY(\vec{R}_{min})]$ as a function of cluster size is shown in Figure 9. Here negative values of $E[Xe_nY(\vec{R}_{min})]$ represent stable clusters while positive values correspond to highly unstable ones. It is clear from these results that in the case of chlorine, the neutral clusters formed after photoionization are bound and stable. However, in the case of bromine the clusters formed, up to $n = 8$, are characterized by a net repulsive potential energy and are expected to be highly unstable.

To study the stability of the clusters formed following the photoionization process, their time evolution was followed using MD simulations. For each cluster 500 trajectories were calculated simulating its time evolution during 100 ps. For the initial conditions we used the coordinates obtained for the lowest energy structure of the ionic clusters, while the initial velocities were sampled from a Boltzmann distribution at 70 K (typical experimental conditions). The fragmentation of the parent clusters following the vertical transition obtained from the MD calculations is summarized in Figure 10. The data present the average size distribution of the fragment clusters at the end of the simulation period. It is clear that the two types of clusters

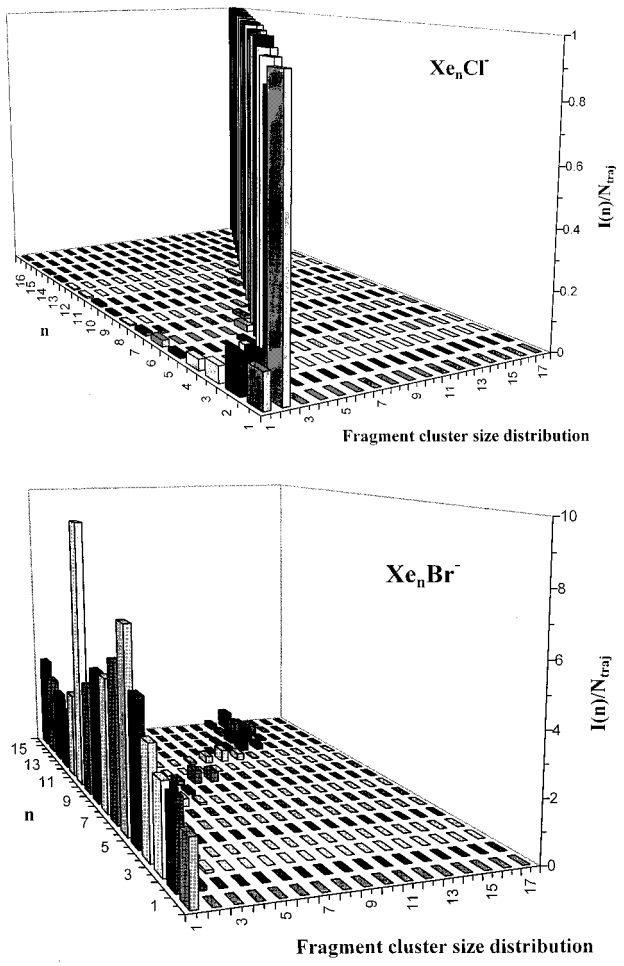

Figure 10. Size distribution of fragment clusters following the photoionization process. Here, $I(n)$ is the number of fragments containing n atoms and N_{traj} is the total number of trajectories calculated.

exhibit markedly different behaviors. In the case of Xe_nCl, for large n values almost no fragmentation occurs during the first 100 ps following the photoionization. For smaller parent clusters, $n < 7$, the emission of single atoms and pairs of atoms is observed; however, most of the original clusters do not split into smaller fragments. These results are consistent with the observations discussed above. Namely, the great similarity between the symmetry and interparticle distances of the lowest energy structures for Xe_nCl^- and Xe_nCl leads to the formation of stable neutral clusters after the photodetachment process. For most n values the excess energy of the newly formed neutral cluster is small and not enough to result in the emission of a fragment cluster during the time examined in the simulations.

The situation is markedly different in the case of Xe_nBr^- clusters. Here, a very high probability of fragmentation is observed for all n values. It is clear that in all cases the emission of atomic fragments is the most probable process, while the formation of larger fragments occurs with low probability. For all cluster sizes in this group, the survival probability of the parent species at the end of the simulation is very low. Namely, all the clusters undergo rapid fragmentation following photoionization; these results clearly demonstrate the high instability of the Xe_nBr clusters formed after photoionization. This finding is in agreement with the above analysis of the origin of E_{stab}, which includes a large contribution from repulsive interactions deriving from cluster deformation.

IV. Summary

A detailed study of the energetics, structures and dynamics of halogen containing (Cl and Br) Xe clusters was described. The lowest energy structures of differently sized clusters (in the range 1−16) of Xe atoms together with ionic and neutral halogen atoms were examined using a GA-based optimization method. The correspondence was established between the structures of these clusters and the bond strength and equilibrium separations of the various pairs of particles in the cluster. We found that in the case of chlorine, the symmetry and interparticle distances in the ionic and neutral clusters are almost identical. However, for Br-containing clusters marked differences between the ionic and neutral systems were observed. Moreover, both Cl^- and Cl were found to be located inside the Xe cluster, while Br^- and Br were found to be attached to the Xe cluster surface. These results were used to evaluate the stabilization energies of the ionic clusters and to assess their relative stability. An analysis of the origin of E_{stab} shows that for Cl^- it corresponds mainly to the difference in binding energies of $Xe-Cl^-$ and Xe−Cl. In the case of bromine, the magnitude of E_{stab} is determined by the difference in the binding of $Xe-Br^-$ and Xe−Br together with a major contribution of repulsive potential energy due to structural distortions. These large differences in E_{stab} for Xe_nCl^- and Xe_nBr^- were shown (using MD simulations) to result in markedly different fragmentation patterns following photoionization.

References and Notes

(1) See, for example: (a) Hoare, M. R.; Pal, P. *Adv. Phys.* **1971**, *20*, 161. (b) Hoare, M. R.; McInnes, J. A. *Adv. Phys.* **1983**, *32*, 791. (c) Garzon, I.; Long, X. P.; Kawai, R.; Weare, J. H. *Chem. Phys. Lett.* **1989**, *158*, 525. (d) Garzon, I.; Long, X. P.; Kawai, R.; Weare, J. H. *Z. Phys. D* **1989**, *12*, 81.

(2) See, for example: (a) Garzon, I. L.; Blaisten-Barojas, E. *Chem. Phys. Lett.* **1986**, *124*, 84. (b) Jonsson, H.; Weare, J. H. *Phys. Rev. Lett.* **1986**, *57*, 412.

(3) See, for example: (a) Wales, D. J.; Berry, R. S. *J. Chem. Phys.* **1990**, *92*, 4283. (b) Perera, L.; Amar, F. G. *J. Chem. Phys.* **1990**, *93*, 4884. (c) Perera, L.; Berkowitz, M. L. *J. Chem. Phys.* **1992**, *96*, 8288. (d) Perera, L.; Berkowitz, M. L. *J. Chem. Phys.* **1993**, *99*, 4222. (e) Perera, L.; Berkowitz, M. L. *J. Chem. Phys.* **1994**, *100*, 3085.

(4) See, for example: (a) Wille, L. T. *Chem. Phys. Lett.* **1987**, *133*, 405. (b) Asher, R. L.; Micha, D. A.; Brucat, P. J. *J. Chem. Phys.* **1992**, *96*, 7683.

(5) See, for example: (a) Celii, F. C.; Janda, K. C. *Chem. Rev.* **1986**, *86*, 507. (b) Castleman, A. W.; Keese, R. G. *Acc. Chem. Res.* **1986**, *19*, 413. (c) Castleman, A. W.; Keese, R. G. *Chem. Rev.* **1986**, *86*, 589. Hiraoka, K.; Mizuse, S.; Yamabe, S. *J. Phys. Chem.* **1988**, *92*, 3943.

(6) See, for example: (a) Amirav, A.; Even, U.; Jortner, J. *J. Chem. Phys.* **1981**, *75*, 2489. (b) Hough, T. E.; Miller, R. E.; Scoles, G. *J. Chem. Phys.* **1978**, *69*, 1588. (c) Miller, R. E.; Watts, R. O.; Ding, A. *Chem. Phys.* **1984**, *83*, 155. (d) Brucat, P. J.; Zheng, L.-S.; Pettiette, C. L.; Yang, S.; Smalley, R. E. *J. Chem. Phys.* **1986**, *84*, 3078. (e) Ross, U.; Schultze, Th. *J. Chem. Phys.* **1986**, *85*, 2664. (f) Garvey, J. F.; Bernstein, R. B. *J. Am. Chem. Soc.* **1986**, *108*, 6096. (g) Levandier, D. J.; McCombie, J.; Pursel, R.; Scoles, G. *J. Chem. Phys.* **1987**, *86*, 7239.

(7) See, for example: (a) Leopold, D. G.; Ho, J.; Lineberger, W. C. *J. Chem. Phys.* **1987**, *86*, 175. (b) Ho, J.; Ervin, K. M.; Lineberger, W. C. *Ibid.* **1991**, *93*, 6987. (c) Gantefor, G.; Meiwes-Broer, K. H.; Lutz, H. O. *Phys. Rev. A* **1988**, *37*, 2716. (d) Cheshnovsky, O.; Taylor, K. J.; Conceicao, J.; Smalley, R. E. *Phys. Rev. Lett.* **1990**, *64*, 1785. (e) Markovich, G.; Pollack, S.; Giniger, R.; Cheshnovsky, O. *J. Chem. Phys.* **1994**, *101*, 9344.

(8) (a) Zeiri, Y. *Phys. Rev. E* **1995**, *51*, R2769. (b) Zeiri, Y.; Fattal, E.; Kosloff, R. *J. Chem. Phys.* **1995**, *102*, 1859. (c) Zeiri, Y. *Comput. Phys. Com.* **1997**, *103*, 28.

(9) (a) Niesse, J. A.; Mayne, H. R. *J. Chem. Phys.* **1996**, *105*, 4700. (b) Pullan, W. J. *J. Comput. Chem.* **1997**, *18*, 1096. (c) Gregurick, S. K.; Alexander, M. H.; Hartke, B. *J. Chem. Phys.* **1996**, *104*, 2684.

(10) See, for example: (a) Goldberg, D. E.; *Genetic Algorithms in Search, Optimization, and Machine Learning*; Addison-Wesley: Reading, MA, 1989. (b) Mitchell, M. *An Introduction to Genetic Algorithms*; MIT Press: 1996. (c) Davis, L. *Handbook of Genetic Algorithms* Van Nostrand Reinhold: New York, 1991. (d) *Proceedings of the 3rd International Conference on Genetic Algorithms*; Schaffer, J. D., Ed.; Morgan Kaufman: San Mateo, CA, 1989.

(11) Mansky, E. J.; Flannery, M. R. *J. Chem. Phys.* **1993**, *99*, 1962.

(12) Buck, U. *Adv. Chem. Phys.* **1976**, *30*, 314.

(13) Christoffel, K. M.; Trayanov, A. L.; Prisant, M. G. *J. Chem. Phys.* **1994**, *101*, 4418.

(14) Alimi, R.; Brokman, A.; Gerber, R. B. *J. Chem. Phys.* **1989**, *91*, 1611.

(15) Singer, K.; Taylor, A.; Singer, J. V. L. *Mol. Phys.* **1977**, *33*, 1757.

(16) Hu, X.; Martens, C. C. *J. Chem. Phys.* **1993**, *98*, 8551.